University of Groningen

On the identification of merger debris in the Gaia era

Gomez, Facundo A.; Helmi, Amina; Brown, Anthony G. A.; Li, Yang-Shyang

IMPORTANT NOTE: You are advised to consult the publisher's version (publisher's PDF) if you wish to cite from it. Please check the document version below.

Document Version
Publisher's PDF, also known as Version of record

[Link to publication in University of Groningen/UMCG research database](#)

On the identification of merger debris in the *Gaia* era

Facundo A. Gómez,[1]* Amina Helmi,[1] Anthony G. A. Brown[2] and Yang-Shyang Li[1]

[1]*Kapteyn Astronomical Institute, University of Groningen, PO Box 800, 9700 AV Groningen, the Netherlands*
[2]*Sterrewacht Leiden, Leiden University, PO Box 9513, 2300 RA Leiden, the Netherlands*

ABSTRACT

We model the formation of the Galactic stellar halo via the accretion of satellite galaxies on to a time-dependent semicosmological galactic potential. Our goal is to characterize the substructure left by these accretion events in a close manner to what may be possible with the *Gaia* mission. We have created a synthetic *Gaia* solar neighbourhood catalogue by convolving the six-dimensional phase-space coordinates of stellar particles from our disrupted satellites with the latest estimates of the *Gaia* measurement errors, and included realistic background contamination due to the Galactic disc(s) and bulge. We find that, even after accounting for the expected observational errors, the resulting phase space is full of substructure. We are able to successfully isolate roughly 50 per cent of the different satellites contributing to the 'solar neighbourhood' by applying the mean shift clustering algorithm in energy–angular momentum space. Furthermore, a Fourier analysis of the space of orbital frequencies allows us to obtain accurate estimates of the time since accretion for approximately 30 per cent of the recovered satellites.

Key words: methods: analytical – solar neighbourhood – galaxies: formation – galaxies: kinematics and dynamics.

1 INTRODUCTION

How galaxies form and evolve remains one of the most interesting and challenging puzzles in astronomy. Although a great deal of progress has been made in the last decade many questions remain to be addressed. Both theory and observations are now converging on a key ingredient of this formation process; galaxies such as our own Milky Way seem to have experienced the accretion of smaller objects that have come together thanks to the relentless pull of gravity (e.g. White & Rees 1978).

From the observational side, several new studies have revealed the presence of a large amount of stellar streams in galactic stellar haloes, echoes of ancient as well as recent and ongoing accretion events. These stellar streams have been preferentially found in the outer regions of galaxies. The Sagittarius tidal streams (Ibata, Gilmore & Irwin 1994; Ibata et al. 2001b; Majewski et al. 2003) and the Orphan stream (Belokurov et al. 2007) are just two examples of satellite debris in the Milky Way (see also Newberg et al. 2002; Ibata et al. 2003; Yanny et al. 2003; Belokurov et al. 2006; Grillmair 2006; Starkenburg et al. 2009). The abundant substructures found not only in the halo of M31 (e.g. Ibata et al. 2001a; McConnachie et al. 2009), but also in several haloes of other galax-

ies (e.g. Martínez-Delgado et al. 2008, 2009) are an unambiguous proof that accretion is inherent to the process of galaxy formation.

On the theoretical side, models of the formation of stellar haloes in the Λ cold dark matter (ΛCDM) cosmogony have been able to explain their gross structural properties (e.g. Bullock & Johnston 2005; De Lucia & Helmi 2008; Cooper et al. 2010). In these models, the inner regions of the haloes (including the solar neighbourhood) typically formed first and hence contain information about the most ancient accretion events that the galaxy has experienced (e.g. White & Springel 2000; Helmi, White & Springel 2003; Bullock & Johnston 2005; Tumlinson 2010). Previous studies have predicted that several hundreds kinematically cold stellar streams should be present in the solar vicinity (Helmi & White 1999). However, the identification of these streams is quite challenging especially because of the small size of the samples of halo stars with accurate three-dimensional (3D) velocities currently available. Full phase-space information is necessary because of the very short mixing time-scales in the inner regions of the halo. Some progress has been made towards building such a catalogue but only a few detections have been reported to date (Helmi et al. 1999; Klement et al. 2009; Smith et al. 2009). These have made use of catalogues such as SEGUE (Yanny et al. 2009) and RAVE (Zwitter et al. 2008) in combination with Tycho (Høg et al. 2000) and *Hipparcos* (Perryman et al. 1997). Clearly, this field will only advance significantly with the launch of the astrometric satellite *Gaia* (Perryman et al. 2001). This mission from the European Space Agency will provide accurate measurements of the

*E-mail: gomez@astro.rug.nl

six-dimensional (6D) phase-space coordinates of an extraordinarily large number of stars.[1] Together with positions, proper motions and parallaxes of all stars brighter than $V = 20$, *Gaia* will also measure radial velocities down to a magnitude of $V = 17$.

To unravel the accretion history of the Milky Way requires the development of theoretical tools that will ultimately allow the identification and characterization of the substructure present in the *Gaia* data set. Several authors have studied the suitability of various spaces to isolate debris from accretion events (see e.g. Helmi & de Zeeuw 2000; Knebe et al. 2005; Arifyanto & Fuchs 2006; Font et al. 2006; Helmi et al. 2006; Sharma & Johnston 2009). Recently (McMillan & Binney 2008), followed by Gómez & Helmi (2010, hereafter GH10), showed that orbital frequencies define a very suitable space in which to identify debris from past merger events. In frequency space individual streams from an accreted satellite can be easily identified, and their separation provides a direct measurement of its time of accretion. Furthermore, GH10 showed for a few idealized gravitational potentials that these features are preserved also in systems that have evolved strongly in time. While very promising, these studies have focused on a single accretion event on to a host galaxy. In reality, we expect the Galactic stellar halo to have formed as a result of multiple merger events (where most of its mass should have originated in a handful of significant contributors; see e.g. De Lucia & Helmi 2008; Cooper et al. 2010). As a consequence, it is likely that debris from different satellites will overlap in frequency space, complicating their detection.

In this paper we follow multiple accretion events in a time-dependent (cosmologically motivated) galactic gravitational potential. We focus on how the latest estimates of the measurement errors expected for the *Gaia* mission will affect our ability to recover these events. In particular we study the distribution of stellar streams in frequency space and the determination of a satellite's time since accretion from stellar particles located in a region like the solar neighbourhood. Our paper is organized as follows. In Section 2 we present the details of the *N*-body simulations carried out, as well as the steps taken to generate a mock *Gaia* stellar catalogue. In Section 3 we characterize the distribution of debris in a solar neighbourhood-like sphere in the absence of measurement errors, while in Section 4 we focus on the analysis of the mock *Gaia* catalogue. We discuss and summarize our results in Section 5.

2 METHODS

We model the formation of the stellar halo of the Milky Way using *N*-body simulations of the disruption and accretion of luminous satellites on to a time-dependent galactic potential. We describe first the characteristics of the galactic potential and of the population of satellites, as well as the *N*-body simulations. Finally we outline the steps followed to generate a mock *Gaia* star catalogue.

In this paper we adopt a flat cosmology defined by $\Omega_{\mathrm{m}} = 0.3$ and $\Omega_{\Lambda} = 0.7$ with a Hubble constant of $H(z = 0) = H_0 = 70 \ \mathrm{km \ s^{-1} \ Mpc^{-1}}$.

2.1 The galactic potential

To model the Milky Way potential we chose a three-component system, including a Miyamoto–Nagai disc (Miyamoto & Nagai

Table 1. Parameters of the present day Milky Way-like potential used in our *N*-body simulations. Masses are in $\mathrm{M}_{\odot}$ and distances in kpc.

Disc	Bulge	Halo
$M_{\mathrm{d}} = 7.5 \times 10^{10}$	$M_{\mathrm{b}} = 2.5 \times 10^{10}$	$M_{\mathrm{vir}} = 9 \times 10^{11}$
$r_{\mathrm{a}} = 5.4; r_{\mathrm{b}} = 0.3$	$r_{\mathrm{c}} = 0.5$	$r_{\mathrm{vir}} = 250$
		$c = 13.1$

1975),

$$\Phi_{\mathrm{disc}} = -\frac{GM_{\mathrm{d}}}{\sqrt{R^2 + \left(r_{\mathrm{a}} + \sqrt{Z^2 + r_{\mathrm{b}}^2}\right)^2}}, \tag{1}$$

a Hernquist bulge (Hernquist 1990),

$$\Phi_{\mathrm{bulge}} = -\frac{GM_{\mathrm{b}}}{r + r_{\mathrm{c}}}, \tag{2}$$

and a NFW (Navarro, Frenk & White 1996) dark matter halo,

$$\Phi_{\mathrm{halo}} = -\frac{GM_{\mathrm{vir}}}{r[\log(1+c) - c/(1+c)]} \log\left(1 + \frac{r}{r_{\mathrm{s}}}\right). \tag{3}$$

Table 1 summarizes the numerical values of the parameters at redshift $z = 0$ (Allen & Santillán 1991; Bullock & Johnston 2005; Smith et al. 2007; Sofue, Honma & Omodaka 2009). The circular velocity curve in this model takes a value of $220 \ \mathrm{km \ s^{-1}}$ at 8 kpc from the galactic centre, and is shown in Fig. 1. To model the evolution of the Milky Way potential we allow the characteristic parameters to vary in time. For the dark matter halo, the evolution of its virial mass and its concentration as a function of redshift are given by Wechsler et al. (2002) and Zhao et al. (2003):

$$M_{\mathrm{vir}}(z) = M_{\mathrm{vir}}(z = 0) \exp(-2a_{\mathrm{c}}z), \tag{4}$$

where the constant $a_{\mathrm{c}} = 0.34$ is defined as the formation epoch of the halo, and

$$c(z) = \frac{c(z = 0)}{1 + z}. \tag{5}$$

For the disc and bulge components we follow the prescriptions given by Bullock & Johnston (2005), i.e.

$$M_{\mathrm{d,b}}(z) = M_{\mathrm{d,b}}(z = 0)\frac{M_{\mathrm{vir}}(z)}{M_{\mathrm{vir}}(z = 0)} \tag{6}$$
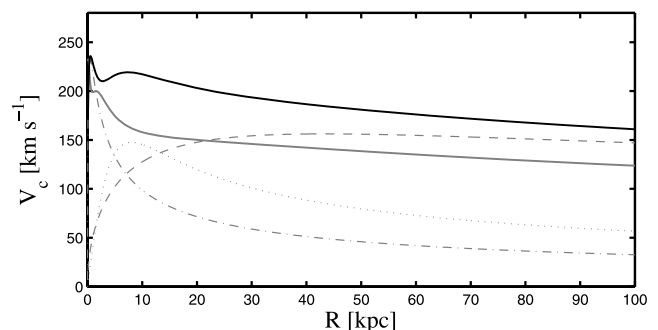

Figure 1. Circular velocity curve as a function of distance from the galactic centre. The thick solid lines represent the total circular velocity used in the suite of simulations at $z = 0$ (black) and $z \sim 1.85$ (grey), respectively. The individual contributions from the dark matter halo, the disc and the bulge at present time are shown by the thin dashed, dotted and dashed–dotted lines, respectively.

for the masses and

$$r_{a,b,c}(z) = r_{a,b,c}(z=0) \frac{r_{vir}(z)}{r_{vir}(z=0)} \tag{7}$$

for the scalelengths. Here r_{vir} is the virial radius of the dark matter halo. Its evolution can be expressed as

$$r_{vir}(z) = \left(\frac{3 M_{vir}(z)}{4 \pi \Delta_{vir}(z) \rho_c(z)} \right)^{1/3}, \tag{8}$$

where $\Delta_{vir}(z)$ is the virial overdensity (Bryan & Norman 1998),

$$\Delta_{vir}(z) = 18\pi^2 + 82[\Omega(z) - 1] - 39[\Omega(z) - 1]^2 \tag{9}$$

with $\Omega(z)$ the mass density of the universe,

$$\Omega(z) = \frac{\Omega_m (1+z)^3}{\Omega_m (1+z)^3 + \Omega_\Lambda}, \tag{10}$$

and $\rho_c(z)$ is the critical density of the universe at a given redshift,

$$\rho_c(z) = \frac{3 H^2(z)}{8 \pi G}, \tag{11}$$

with

$$H(z) = H_0 \sqrt{\Omega_\Lambda + \Omega_m (1+z)^3}. \tag{12}$$

2.2 Satellite galaxies

2.2.1 Internal properties

We assume the properties of the progenitors of our model stellar halo (i.e. the satellites at high redshift) are similar to those at the present day. The Galactic stellar halo has a total luminosity of $\sim 10^9 \, \mathrm{L}_\odot$. To obtain a population of satellites that, after accretion, produces a stellar halo with this total luminosity, we use the luminosity distribution function of the Milky Way satellites given by Koposov et al. (2008):

$$\frac{dN}{dM_V} = 10 \times 10^{0.1(M_V + 5)}. \tag{13}$$

Fig. 2 shows the luminosity function of our model satellite population obtained by randomly drawing 42 objects.
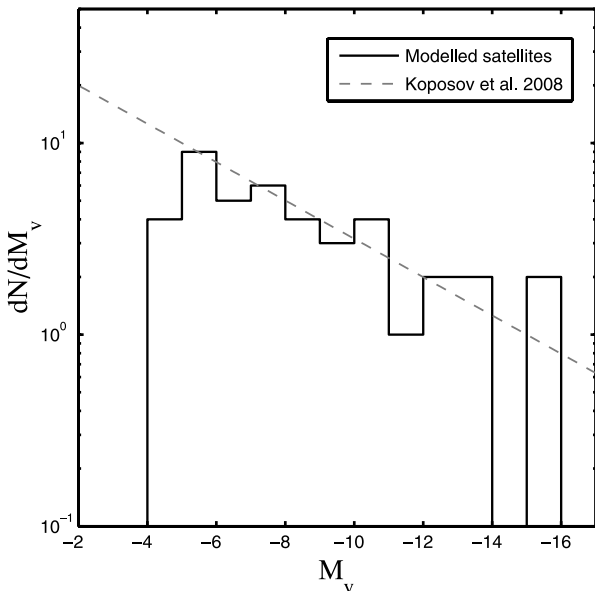

Figure 2. Luminosity function for the model satellite galaxies used in this suite of simulations (histogram). The (grey) dashed line shows the 'all sky SDSS' luminosity function by Koposov et al. (2008).

For the initial stellar structure of the satellites, we assume a King profile (King 1966) with a concentration parameter $c \approx 0.72$. We derive the structural parameters for each of our satellites using the scaling relations

$$\log \frac{L}{L_\odot} - 3.53 \log \frac{\sigma_v}{\mathrm{km\,s^{-1}}} \approx 2.35,$$

$$\log \frac{\sigma_v}{\mathrm{km\,s^{-1}}} - 1.15 \log \frac{R_c}{\mathrm{kpc}} \approx 1.64,$$

as given by Guzmán, Lucey & Bower (1993) for the Coma cluster dwarf elliptical galaxies. Here R_c is the core radius of the King profile, and σ_v is the central velocity dispersion. We note that the total mass of the King model as defined by these parameters may differ from that implied by the satellite's luminosity L. Therefore we also implicitly allow the presence of dark matter in our model satellites. The corresponding (total) mass-to-light ratios for our satellites would range from ~ 250 for the faintest object ($M_V = -5$) to ~ 37 for the brightest one ($M_V = -15.9$).

2.2.2 Orbital properties

The density profile of the stellar halo is often parametrized in a principal axis coordinate system as

$$\rho(x, y, z) = \rho_0 \frac{[x^2 + (y^2/p^2) + (z^2/q^2) + a^2]^n}{r_0^n}, \tag{14}$$

where n is the power-law exponent, p and q the minor- and intermediate-to-major axis ratios, a the scale radius and ρ_0 the stellar halo density at a radius r_0. (See Helmi 2008, for a complete review of recent measurements of these parameters.) Here for simplicity, we shall assume $a = 0$ (as the halo appears to be rather concentrated), $p = q = 1$ and $n = -3$. At the solar radius, $r_0 = \mathrm{R}_\odot = 8 \, \mathrm{kpc}$, ρ_0 corresponds to the local stellar halo density. In this paper we adopt $\rho_0 = 1.5 \times 10^4 \, \mathrm{M}_\odot \, \mathrm{kpc}^{-3}$, as given by Fuchs & Jahreiß (1998).

From this density profile we randomly draw positions at redshift $z = 0$ for the guiding orbit of each one of our satellites. To generate their velocities we follow the method described in section 2.1 of Helmi & de Zeeuw (2000). The main assumption made is that the stellar halo can be modelled by a radially anisotropic phase-space distribution function, which is only a function of energy, E, and angular momentum, L.

This combined set of orbital initial conditions guarantees that at $z = 0$, the observed stellar halo density profile and velocity ellipsoid at the solar radius are roughly matched by our model. These initial conditions are then integrated backwards in time for $\sim 10 \, \mathrm{Gyr}$ ($z \approx 1.85$) in the time-dependent potential described in Section 2.1. Therefore, we now have obtained the set of initial positions and velocities required for forward integration in time of our N-body simulations.

We do not include any numerical treatment of dynamical friction in our simulations. Therefore, and to mimic the effects of this process, we have assigned the five most bound orbits at the present time to the five most massive satellites. For the rest of the satellites the orbits are assigned randomly.

2.2.3 Numerical treatments

The numerical simulations are, in most cases, self-consistently evolved using the massively parallel TREESPH code GADGET-2.0 (Springel 2005). The number of particles used to simulate each

satellite depends on its total luminosity, as explained below (Section 2.3). This number ranges from a minimum of 2.56×10^5 up to 10^7 particles. To avoid very large computational times we neglect self-gravity for the five most massive satellites. We do not expect this to significantly affect our results since these satellites inhabit the inner regions of the host (see Section 2.2.2) and therefore they are rapidly disrupted. For the gravitational softening parameter we choose $\epsilon = 0.025 R_c$ (where R_c is the core radius of the system). After allowing each satellite to relax in isolation for 3 Gyr, we launch it from the apocentre of its orbit and let it evolve for $\sim$10 Gyr under the influence of the time-dependent galactic potential.

2.3 Generating a mock *Gaia* catalogue

2.3.1 N-body particles to stars

To generate a mock *Gaia* catalogue we need to 'transform' our N-body particles into 'stars'. Therefore we assign absolute magnitudes, colours and spectral types to each particle in our simulations. We use the IAC-STAR code (Aparicio & Gallart 2004) which generates synthetic colour–magnitude diagrams (CMDs) for a desired stellar population model. As output we obtain the M_V and $(V - I)$ colour for each stellar particle.

We assign to each satellite a stellar population model (Pietrinferni et al. 2004) with a range of ages from 11 to 13 Gyr, $-2 \le$ [Fe/H] $\le$ -1.5 dex, $[\alpha/\text{Fe}] = 0.3$ and a Kroupa initial mass function (Kroupa, Tout & Gilmore 1993). All these parameters are consistent with the observed values in the Galactic stellar halo (Helmi 2008, and references therein). An example of the resulting CMD is shown in Fig. 3.

Because of the limited resolution of our N-body simulations it is not possible to fully populate the CMDs of our satellites. Therefore each satellite is populated only with stars brighter than $M_V \approx 4.5$, which corresponds to an apparent magnitude $V = 16$ at 2 kpc from the Sun. This choice represents a good compromise between the
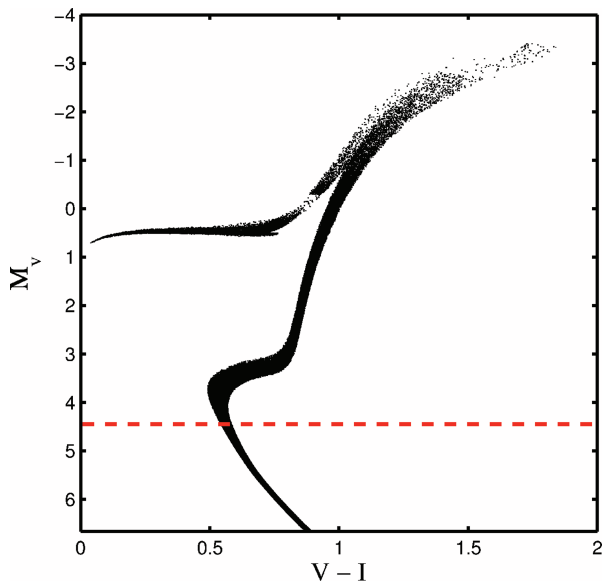
numerical resolution of our simulations and the limiting apparent magnitude V_{lim} for which *Gaia* will measure full 6D phase-space coordinates (astrometric and photometric measurements extend to $V = 20$, but spectroscopic measurements reach $V \approx 17$).

As explained in Section 2.2.1 different satellites have different total luminosities and, thus, the number of stars down to magnitude $M_V \approx 4.5$ varies from object to object. Therefore, in each satellite a different number of N-body particles is converted into stars. To estimate this number we use the CMD code by Marigo et al. (2008), which provides a stellar luminosity function normalized to the initial stellar mass of a given population. The age and metallicity of the stellar population model are fixed to the average values described above and the initial mass is set by the total luminosity of each satellite. Finally, accumulating the number of stars down to $M_V \approx 4.5$ we obtain the number of N-body particles that need to be transformed into stars. This number ranges from 660 for the faintest satellite ($M_V = -5$) to 1.4×10^7 for the brightest one ($M_V = -15.9$).

2.3.2 Disc and bulge contamination

The *Gaia* catalogue will contain not only stars from the halo, but also stars associated to the different components of the Galaxy. These stars act as a *smooth* Galactic background which could in principle complicate the task of identification of debris associated to accretion events. To take into account this stellar background, Brown, Velásquez & Aguilar (2005, hereafter BVA05) created a Monte Carlo model of the Milky Way. This model consists of three different components: a disc, a bulge and a smooth stellar halo; where the latter was meant to take into account the set of halo stars formed *in situ*. In this work we only consider the background contamination by the disc and bulge components of the Monte Carlo Galactic model of BVA05, since we build our stellar halo completely from disrupted satellites. The disc model consists of particles distributed in space according to a double exponential luminosity profile with a scalelength and height of 3.5 and 0.2 kpc, respectively. For the bulge model a Plummer density distribution (Plummer 1911) with a scale radius of 0.38 kpc is adopted. Although the models for the disc luminosity profile and for its gravitational potential (see Table 1) are not self-consistent, the values of the corresponding scales were chosen in an attempt to faithfully match (i) the observed stellar density at the location of the Sun and (ii) the Galactic circular velocity profile. To each particle an absolute magnitude and spectral class is assigned according to the Hess diagram listed in tables 4–7 of Mihalas & Binney (1981). Finally, the kinematics are modelled assuming different velocity ellipsoids for stars in the disc of each spectral type whereas an isotropic velocity dispersion is assumed for bulge stars. For more details, see section 2.1 of BVA05.

2.3.3 Adding Gaia errors

To convolve the positions and velocities of our mock catalogue of stars with the expected *Gaia* errors we have followed the steps described in section 4.1 of BVA05. Here we give a short overview of the procedure but we refer the reader to BVA05 for more details. As a first step, we transform Galactocentric positions and velocities to heliocentric coordinates, $r_{\text{helio}} = r_{\text{gal}} - r_\odot$ and $v_{\text{helio}} = v_{\text{gal}} - v_\odot$. Subsequently, these quantities are transformed into radial velocity and five astrometric observables that

Figure 3. Example of a synthetic CMD used to populate our model satellite galaxies with 'stars'. The stellar population model (Pietrinferni et al. 2004) used has a range of ages from 11 to 13 Gyr, $-2 \le$ [Fe/H] ≤ -1.5 dex, $[\alpha/\text{Fe}] = 0.3$ and a Kroupa initial mass function (Kroupa et al. 1993). The dashed line indicates the limiting absolute magnitude considered in our simulations ($M_V \approx 4.5$).
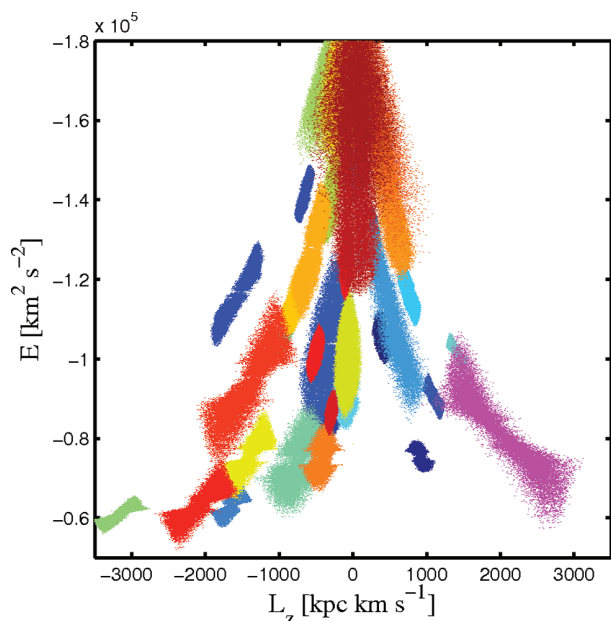
Figure 4. Distribution of particles in $E - L_z$ space after 10 Gyr of evolution. Different colours represent different satellites.

Gaia will measure, i.e. the Galactic coordinates (l, b), the parallax ϖ and the proper motions $\mu_{l*} = \mu_l \cos b$ and μ_b. The next step consists in convolving with the expected *Gaia* errors according to the accuracy assessment described in the *Gaia* web pages at ESA (http://www.rssd.esa.int/gaia). Note that the errors vary most strongly with apparent magnitude, with a weaker dependence on colour and position on the sky. Finally, we transformed the particles' observed phase-space coordinates back to the Galactocentric reference frame for our analysis.

3 CHARACTERIZATION OF SATELLITE DEBRIS

In this section we analyse how the debris of our 42 satellites is distributed in various projections of phase space, before taking into account how the *Gaia* observations will affect this distribution. In comparison to previous works (e.g. Helmi & de Zeeuw 2000), recall that our satellites have evolved in a live potential for 10 Gyr.

3.1 Traditional spaces

Fig. 4 shows the distribution of $\sim 2.5 \times 10^4$ randomly chosen particles from each satellite in the space of energy, E, and the z-component of the angular momentum, L_z. The different colours represent different satellites. Note that in this projection of phase space a large amount of substructure is still present, despite the strong evolution of the host gravitational potential (e.g. the total mass increased by a factor of ~ 3.5).

We focus now on the stellar particles from our mock *Gaia* catalogue (prior to error convolution) located within a 'solar neighbourhood' sphere of 2.5-kpc radius, centred at 8 kpc from the galactic centre. Figs 5 and 6 show their distribution on the sky and in velocity space, respectively. Inside this sphere we find approximately 2×10^4 stellar particles coming from 22 different satellites that contribute with, at least, 20 stars brighter than $M_V \approx 4.5$. The distribution on
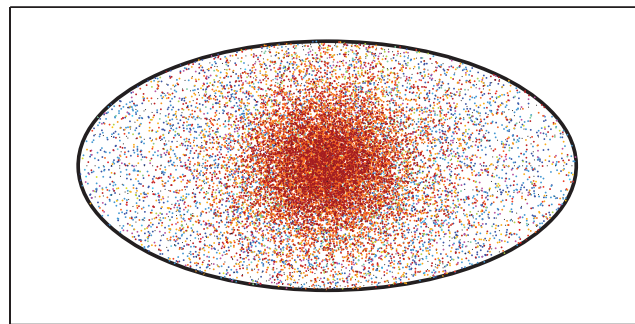

Figure 5. Distribution on the sky (l, b) of the stellar particles located inside a sphere of 2.5-kpc radius centred at 8 kpc from the galactic centre. Different colours represent different satellites.

the sky is very smooth[2] and, thus, disentangling merger debris in the 'solar neighbourhood' by only using spatial information is not obvious. On the contrary, substructure can be observed in velocity space but this is clearly less sharply defined than what is found in the pseudo-integrals of motion $E - L_z$ space (e.g. Fig. 4). We turn next to the space of orbital frequencies where we also expect to find much clumpiness.

3.2 Frequency space

The orbital frequencies of the stellar particles are computed as follows (see also section 5.1 of GH10).

(i) We assume a fixed underlying potential as described in Section 2.1 at $z = 0$.

(ii) We integrate the orbits of each stellar particle for approximately 100 orbital periods.

(iii) We obtain their orbital frequencies by applying the spectral analysis code developed by Carpintero & Aguilar (1998).

3.2.1 Generalities

The distribution of the stellar particles in frequency space is shown in the left-hand panel of Fig. 7. We use the same colour coding as in previous figures. Note that satellite galaxies do not appear as a single and smooth structure, but rather as a collection of well-defined and small clumps. These small clumps are associated to the different stellar streams crossing our solar neighbourhood sphere at the present time. In a time independent gravitational potential, streams are distributed in frequency space along lines of constant Ω_r and Ω_ϕ. However, in a time-dependent potential, such as the one considered here, streams are distributed along lines with a given curvature, which itself depends upon the rate of growth of the potential (see also GH10).

The left-hand panel of Fig. 7 also shows that in the Ω_ϕ versus $\Omega_r - \Omega_\phi$ space satellites may strongly overlap. This situation can be considerably improved by adding the z-component of the angular momentum as an extra dimension to this space, as shown in the right-hand panel of Fig. 7.

The distribution of debris in the space of $\Omega_r - \Omega_\phi$ versus L_z is very similar to that in E versus L_z, as a coarse comparison between Figs 4 and 7 will reveal. Note as well that as in $E - L_z$ space, from this

---

[2] The central overdensity is merely due to the increase in stellar halo density towards the Galactic centre.
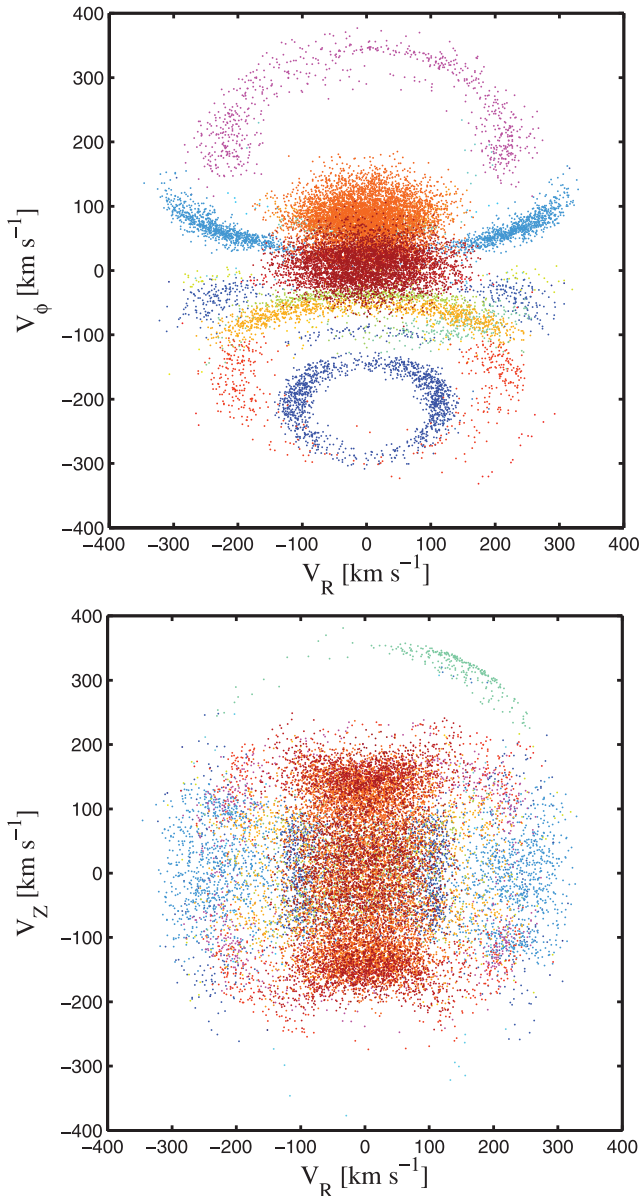
Figure 6. Distribution in two different projections of velocity space of the stellar particles shown in Fig. 5.

projection it is possible, solely by eye inspection, to isolate a few accreted satellites.

From this figure we can also notice that satellites on low-frequency orbits have a smaller amount and a set of better-defined streams than those on orbits with high frequency. The reason for this is twofold. First, satellites on low-frequency orbits spend most of their time far from the centre of the host potential and therefore have longer mixing time-scales, as opposed to those on high-frequency orbits (short periods). Secondly, potentials such as the one considered in this work may admit a certain degree of chaoticity (e.g. Schuster & Allen 1997). Satellites on highly eccentric short-period orbits come close to the galactic centre and may be 'scattered' via chaos. Such chaotic orbits do not have stable fundamental frequencies (since they have fewer integrals of motion than needed and thus wander through phase space). Therefore, their structure in frequency space is rapidly erased.

It is important to note that our desire to analyse a 'solar neighbourhood' sphere has resulted in certain limitations. For example, some satellites do not contribute at all to this volume because of their particular orbit. In addition, most of the faint satellite galaxies have only a few, if any, 'stars' with absolute magnitude above the limiting magnitude of our mock *Gaia* catalogue and therefore they are not 'observable', either.

3.2.2 Estimating the time of accretion

An important feature of frequency space is that an estimate of the time since accretion of a satellite can be derived by measuring the separation between adjacent streams along the Ω_ϕ or Ω_r directions (McMillan & Binney 2008; GH10). This characteristic scale may be estimated through a Fourier analysis technique as follows.

(i) We create an image of the scatter plot in frequency space, by griding the space with a regular $N \times N$ mesh of bin size Δ and count the number of stellar particles in each bin.

(ii) We apply a 2D discrete Fourier Transform to this image and obtain $H(k_r, k_\phi)$.

(iii) We compute a 1D power spectrum along a thin slit centred on the wavenumbers $k_r/(N\Delta), k_\phi/(N\Delta) = 0$ as

$$P(0) = \frac{1}{N^2} |H(0, 0)|^2,$$

$$P(k_\phi) = \frac{1}{N^2} \left[|H(k_\phi, 0)|^2 + |H(-k_\phi, 0)|^2 \right]$$

for $k_\phi = 1, \ldots, \left(\frac{N}{2} - 1 \right),$

$$P(N/2) = \frac{1}{N^2} |H(-N/2, 0)|^2 \qquad (15)$$

and analogously for $P(k_r)$.

(iv) We identify the wavenumber f_0 of the dominant peak in the spectra, which corresponds to a wavelength equal to the distance between adjacent streams in frequency space.

(v) The estimate of the time since accretion is $\tilde{t}_{acc} = 2\pi f_0$ (for more details, see section 3.2.3 of GH10).

We have applied this method to three different satellites from our simulations. Two of these satellites (labelled number 1 and 2 in the right-hand panel of Fig. 7) have a low-frequency guiding orbit and, just by eye inspection, can be isolated in L_z versus $\Omega_r - \Omega_\phi$ space. The third one (number 3) has a high frequency guiding orbit and overlaps with some other satellites in this space.

In Fig. 8 we zoom into the distribution of particles in frequency space for each satellite separately. From this figure we clearly appreciate the large number of streams that each of these satellites is contributing to this 'solar neighbourhood' volume. Although the number of streams apparent in this figure is very large (44, 30 and 59, for satellite 1, 2 and 3, respectively), this is consistent with the models of Helmi & White (1999), who predicted a total of ~300–500 streams locally, i.e. in an infinitesimal volume around the Sun. This is encouraging particularly because the models presented here are more realistic than those by Helmi & White (1999).

To obtain an estimate of the time since accretion for our satellites we compute the normalized power spectrum along the $k_r = 0$ direction. The results are shown in the bottom panels of Fig. 8. From left to right, the peak with the highest amplitude in the spectrum is located at a wavenumber of $f_0 = 1.24, 1.41$ and 1.21 Gyr, respectively. These values correspond to an estimated time since accretion
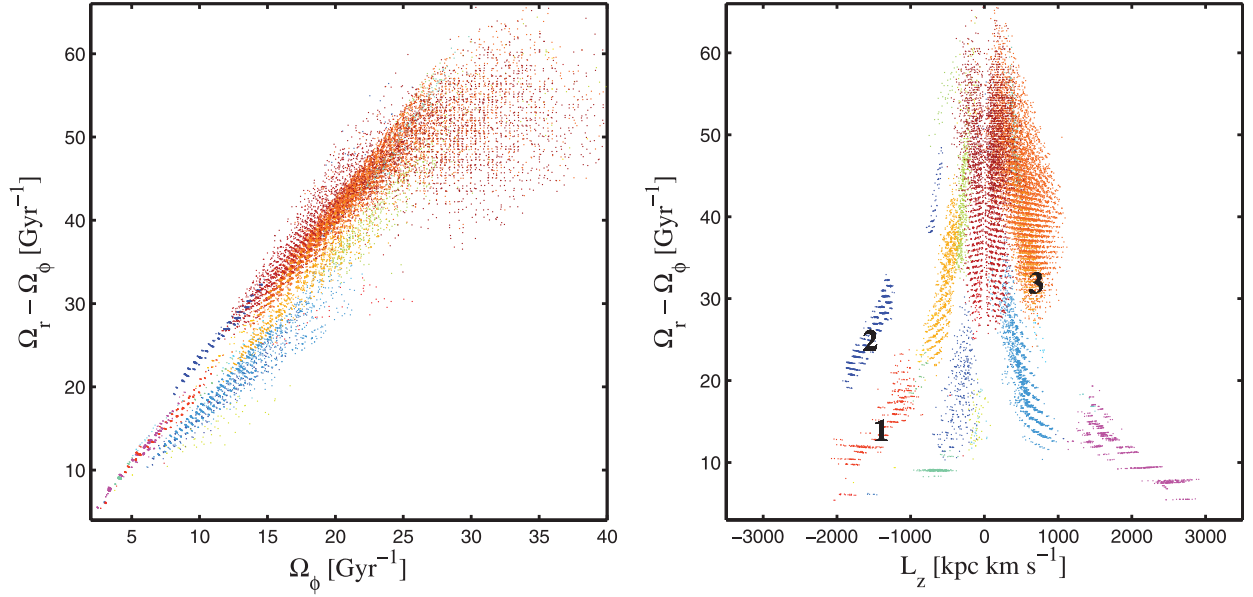
Figure 7. Distribution of stellar particles in frequency (left-hand panel) and L_z versus $\Omega_r-\Omega_\phi$ (right-hand panel) space located inside a sphere of 2.5-kpc radius at 8 kpc from the galactic centre. The colour coding is the same as in previous figures. Note that this distribution of particles was obtained without taking into account the expected *Gaia* observational errors.
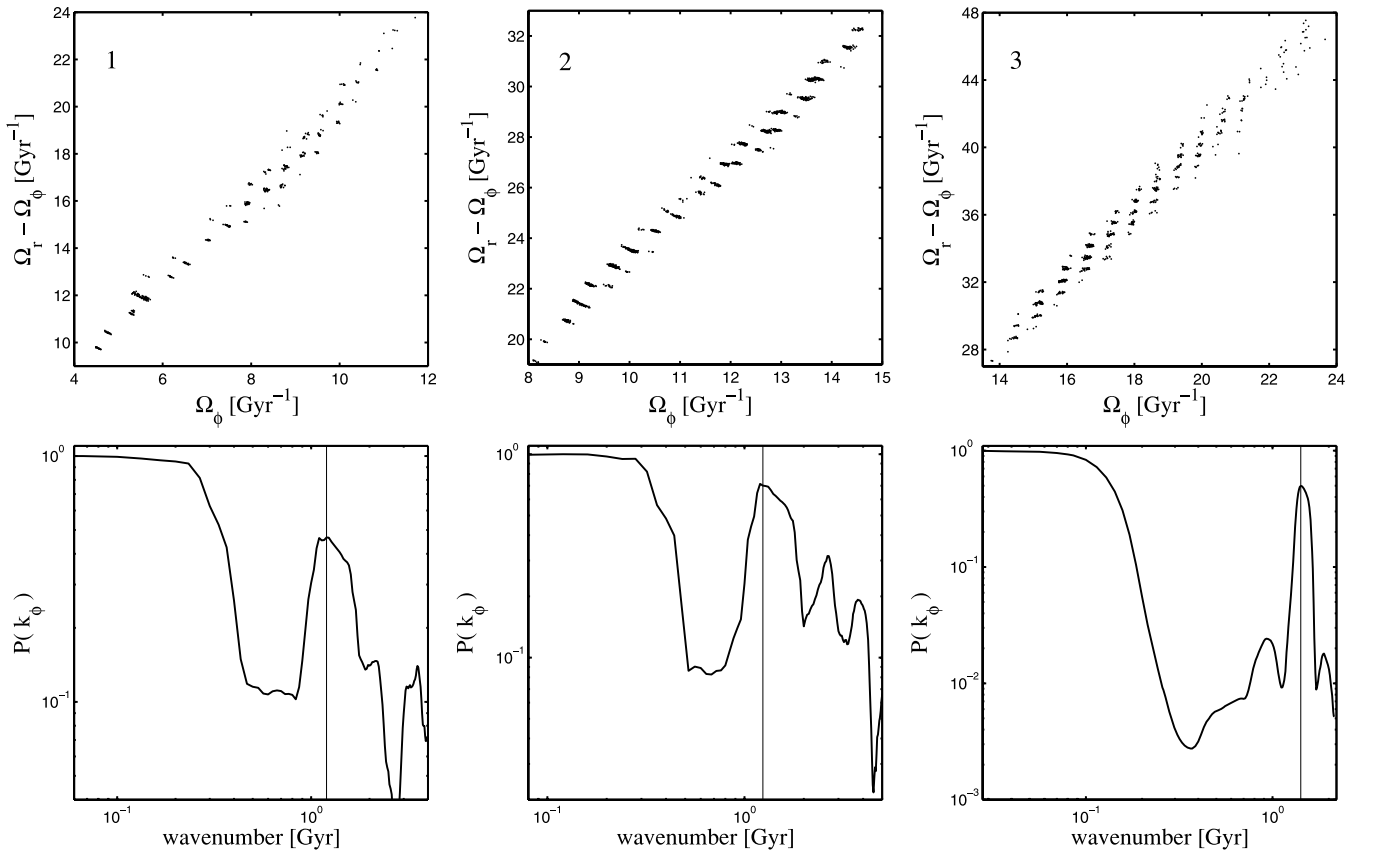

Figure 8. The top panels show for three different satellites, the distribution of stellar particles in frequency space located inside a sphere of 2.5-kpc radius at 8 kpc from the galactic centre. The bottom panels show the 1D normalized power spectra along the $k_r = 0$ direction, obtained as explained in Section 3.2.2. The wavenumber of the dominant peak (denoted by the vertical lines in these panels) is used to estimate the accretion time of the satellites. Other peaks in the spectra are associated to either the harmonics of this wavenumber or to the global shape of the particle's distribution in frequency space.

of 7.8, 8.9 and 7.6 Gyr, respectively. These are in reasonable agreement with the true value, which we define as the time when 80 per cent of the stellar particles became unbound.[3] For each satellite we obtain a t_{acc} of 9, 9.4 and 9.7 Gyr, respectively. In agreement with GH10, we find that this method provides a lower limit to the actual time since accretion, differing by 15–25 per cent. This is very encouraging since GH10 did not study such a complex growth of the host potential.

4 ANALYSIS OF THE MOCK *GAIA* CATALOGUE

We will now analyse the phase-space distribution of stellar particles located in a volume in the 'solar neighbourhood', as may be observed in the future by *Gaia*. We study how the *Gaia* errors, as well as the contamination from other Galactic components, would affect our ability to identify and characterize merger debris.

4.1 Contamination by disc and bulge

As in Section 3.2, we restrict our analysis to the stellar particles located inside a sphere of 2.5-kpc radius centred at 8 kpc from the galactic centre. To account for the maximum possible degree of background contamination, we consider all the stars for which *Gaia* will measure full phase-space coordinates (i.e. all stars brighter than $V = 17$), according to the Monte Carlo model of the disc and bulge.

Disc particles largely outnumber those in the stellar halo, generally providing a prominent background. However much of this can be removed by considering the metallicity distribution function (MDF) of the Galactic components. While the MDF of the halo peaks at approximately $[Fe/H] = -1.6$, that of disc peaks at $[Fe/H] \approx -0.2$. As a consequence, stars from the disc are in general more metal rich and therefore a simple cut on metallicity could be of great help to isolate halo stars in our sample.

It is therefore important to characterize well the metal-poor tail of the Galactic disc MDF. We use the model by Ivezić et al. (2008) to represent this tail:

$$p(x) = G_1(x|\mu_1, \sigma_1) + 0.2 \, G_2(x|\mu_2, \sigma_2), \quad x = [Fe/H] \quad (16)$$

and

$$G(x|\mu, \sigma) = \frac{1}{\sqrt{2\pi}\sigma} \exp \frac{-(x-\mu)^2}{2\sigma^2}. \quad (17)$$

Here $\sigma_1 = 0.16$ dex, $\sigma_2 = 0.1$ dex, $\mu_2 = -1.0$. Ivezić et al. (2008) found μ_1 to vary as a function of the height from the plane of the disc, but for simplicity we fix $\mu_1 = -0.71$. The contribution of stars more metal rich than $[Fe/H] \approx -0.4$ to the study of Ivezić et al. (2008) is small (because of a restriction imposed on the colour range). Therefore to account for this population in our model, we normalize $p([Fe/H])$ with a constant α. The numerical value of α is such that at its peak value (located at $[Fe/H] \approx -0.7$) $p([Fe/H])$ matches the MDF of the Geneva–Copenhagen survey (Nordström et al. 2004).

Having derived a MDF for our disc model, we can proceed to apply a cut on metallicities $[Fe/H] \geq -1.1$ to the disc particles present in our 'solar neighbourhood' sphere of 2.5-kpc radius. Although in our simulation halo stars have metallicities between $-2.0 \leq [Fe/H] \leq -1.5$, stars with higher metallicities are known

to be present in the Galactic stellar halo. Hence the more generous cut. This cut leads to a subsample of only $\approx 9.3 \times 10^3$ 'disc stars' brighter than $V = 17$ out of a total of 4.1×10^7 found in our model.

A similar approach can be followed for the bulge component. In this case metallicities are assigned according to the observed MDF of the Galactic bulge, as given by Zoccali (2009). This MDF is modelled as a single Gaussian distribution with a mean metallicity $\langle[Fe/H]\rangle = -0.28$ dex and a dispersion $\sigma = 0.4$ dex, as found in the outermost field analysed by Zoccali (2009) (located at a latitude of $b = -12°$).

After removing all stellar particles with $[Fe/H] \geq -1.1$, out of the 2.9×10^4 bulge stellar particles with $V \leq 17$ originally present in our 'solar neighbourhood' sphere we are left with only 784 stars. This very small number suggests that the contamination from this Galactic component should not strongly affect the detection of substructure in phase space.

4.2 Frequency space

Fig. 9 shows the distribution of stellar particles inside the 'solar neighbourhood' sphere in both frequency (left-hand panel) and L_z versus Ω_r–Ω_ϕ (right-hand panel) space, now after error convolution. Again, the different colours indicate stellar particles from different satellites, with the addition of the disc and bulge which are shown in black. Interestingly, in both spaces disc particles are part of a very well defined and quite isolated structure since, as expected for stars moving in the galactic plane on a circular orbit, they have the largest values of $|L_z|$ at a given Ω_r–Ω_ϕ. Therefore, it is possible to isolate and easily eliminate the contamination from the disc. On the other hand, bulge particles are sparsely distributed in both spaces and, although there are very few, they cannot be isolated simply as in the case of the disc. None the less, they do not define a clump that could be confused with merger debris.

Both panels of Fig. 9 show that, even after convolution with the latest model of the *Gaia* measurement errors, significant substructure is apparent in L_z versus Ω_r–Ω_ϕ versus Ω_ϕ space. Comparison to Fig. 7 shows very good correspondence between clumps, although these are, as a consequence of the convolution, generally less well defined and contain less internal substructure.

4.2.1 Estimating the time since accretion

A derivation of the time since accretion is significantly more difficult when the *Gaia* measurement errors are taken into account. We exemplify this by focusing on the three satellites described in Section 3.2.2. The 'observed' distribution of stellar particles in frequency space is shown in grey in the top panels of Fig. 10. A direct comparison to Fig. 8 clearly highlights what the effects of the *Gaia* errors are. As in Section 3.2.2, we perform our Fourier analysis and compute the normalized power spectra. These are shown with a black solid line in the bottom panels of Fig. 10. Only for the spectrum shown in the middle panel we can identify a single dominant peak. Therefore observational errors seem to be large enough to erase the signal associated with the time since accretion in the power spectrum for at least some of our satellite galaxies.

We wish to obtain an order of magnitude estimate of how large the errors in velocities have to be to blend two adjacent streams in frequency space. Let us consider a satellite moving on a circular orbit accreted $t_{acc} = 8$ Gyr ago. The separation of two adjacent streams in frequency space is $\Delta\Omega = 2\pi/t_{acc} \approx 0.78$ (comparable to that found for the satellites in our simulations). Since $V_\phi = R\Omega$,

---

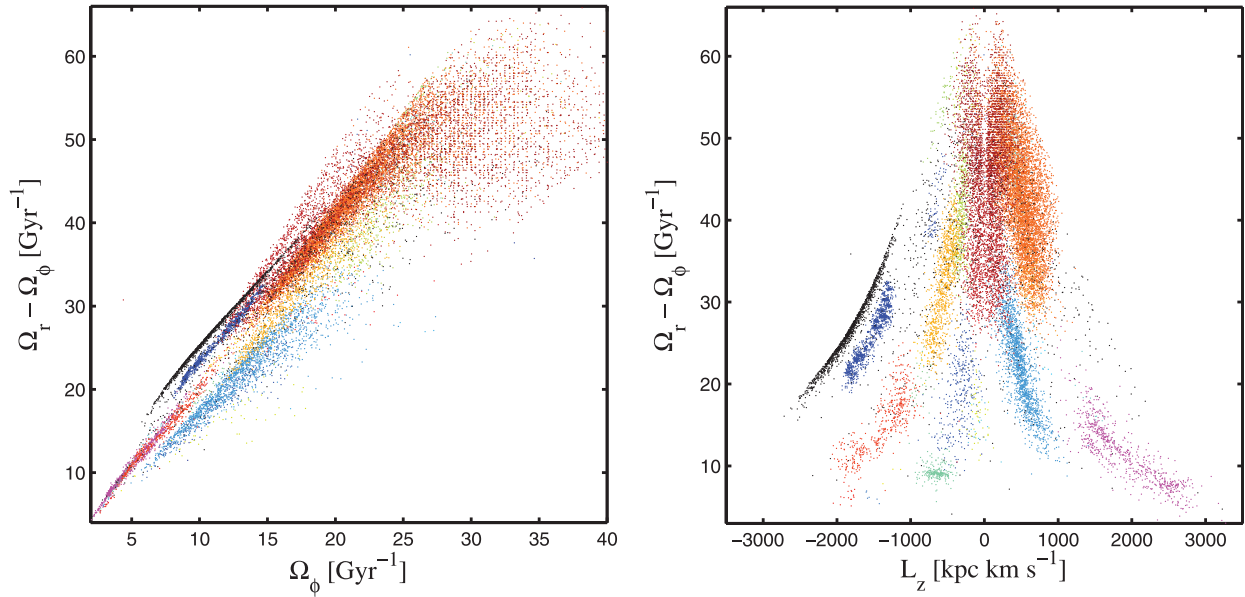[3] For simplicity we assume that a particle becomes unbound when it is found outside the initial satellite's tidal radius, obtained from the initial King profile.

Figure 9. Distribution of stellar particles in frequency (left-hand panel) and L_z versus $\Omega_r-\Omega_\phi$ (right-hand panel) space located inside a sphere of 2.5-kpc radius at 8 kpc from the galactic centre, after convolution with the *Gaia* observational errors. The black dots denote the contribution from the disc and bulge. The rest of the colours represent different satellites.
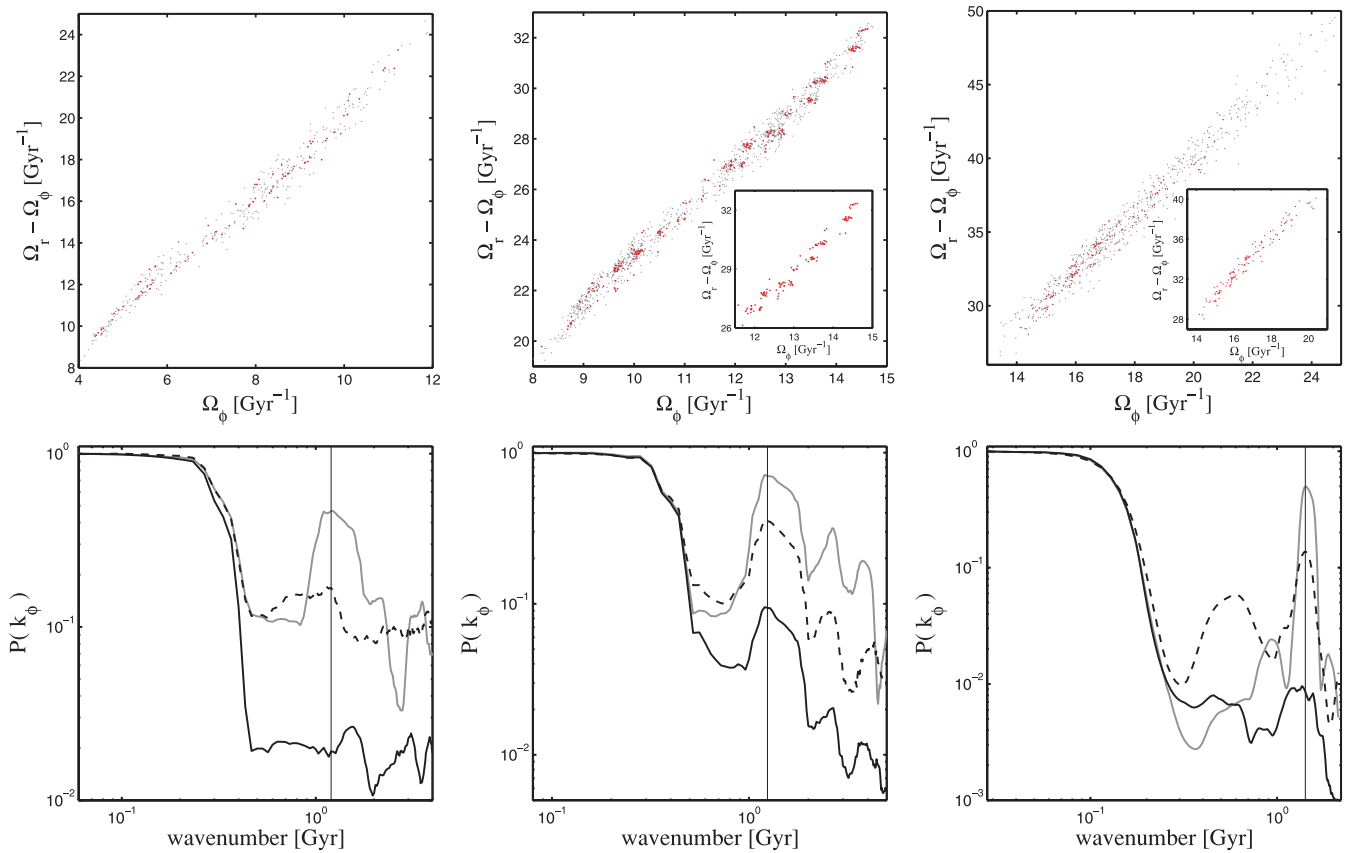

Figure 10. Top panels: distribution of stellar particles in frequency space for the three satellites shown in Fig. 8, after convolution with the *Gaia* observational errors. Grey dots show the distribution of all the stellar particles inside the 'solar neighbourhood' sphere, whereas the red dots are the subset with $\sigma_\varpi/\varpi \leq 0.02$ (see also zoom-in). Bottom panels: the black solid lines show the 1D normalized power spectra obtained from the distribution of points shown in the top panels, while the black dashed lines correspond to the subset with $\sigma_\varpi/\varpi \leq 0.02$. The grey solid lines show the normalized power spectra obtained from the distribution of particles before convolution with the observational errors (cf. Fig. 8). Their largest amplitude peak is indicated with a vertical line.

we may deduce that the maximum error in the tangential velocity should be $\sigma_{v_\phi} = R\Delta\Omega$. Therefore, for the streams found at $R = 8$ kpc from the Galactic centre, $\sigma_{v_\phi} \leq 6$ km s^{-1}. This implies that, to be able to estimate the time since accretion from the power spectra, the relative parallax errors should be[4] $\sigma_\varpi/\varpi \leq 0.02$.

The set of stellar particles from each of our three satellites satisfying this condition is shown as red dots in the top panel of Fig. 10. Out of the 445 (left-hand panel), 1264 (middle panel) and 720 (right-hand panel) stellar particles originally found inside our solar neighbourhood sphere, only 90, 239 and 113, respectively, have remained after the error cut. The normalized power spectra obtained for these distributions are shown with dashed black lines in bottom panels of Fig. 10. Now, the largest amplitude peak is (once again and for all satellites) associated with the time since accretion. Note that, since each peak is located at the same wavenumber as in the analysis with no observational errors (grey curves in this figure), the estimated times since accretion for each satellite are exactly those obtained in Section 3.2.2.

Nevertheless, it is clear that the signal found in the power spectra could be determined better if a larger number of stars with $\sigma_\varpi/\varpi \leq 0.02$ were available. Such stars are expected to be present in the *Gaia* catalogue, but because of the limited numerical resolution of our experiments, they are not part of our mock *Gaia* catalogue. Such stars would be fainter than $M_V = 4.5$, but closer than 2 kpc from the Sun. For example, according to the latest *Gaia* performance numbers, a dwarf star located at 1 kpc from the Sun, with an apparent magnitude of $V \approx 16$ should have a parallax measurement error $\sigma_\varpi/\varpi \leq 0.02$. This apparent magnitude and distance translates into an absolute magnitude of $M_V \approx 6$, i.e. it is 1.5 mag fainter than limiting magnitude we have used in our simulations. If we use the number of particles found at distances closer than 1 kpc from the Sun, and if we take into account the luminosity functions of the three satellites in Fig. 10, we can obtain an estimate of how many stars would be observable by *Gaia* with the desired parallax errors. In this way we find, respectively, 186, 465 and 276 extra stars with $4.5 \leq M_V \leq 12$, which would thus allows to estimate the time since accretion for each satellite.

4.3 Identification of satellites

Although promising, this is unlikely to be the way we will proceed in the future with real *Gaia* observations. In order to obtain an estimate of the time since accretion of any given satellite, we first have to efficiently identify it. This can be achieved by applying a suitable clustering technique. In this work we have used the mean shift algorithm (Fukunaga & Hostetler 1975; Comaniciu & Meer 2002; Derpanis 2005). The main idea behind mean shift is to treat the points in any N-dimensional space as an empirical probability density function where dense regions in the space correspond to the local maxima of the underlying distribution. For each data point in the space, one performs a gradient ascent procedure on the local estimated density until convergence is reached. Furthermore, the data points associated with the same stationary point are considered members of the same cluster.

We have applied the mean shift algorithm to the set of particles inside a sphere of 4-kpc radius, located at 8 kpc from the galactic

centre, projected into the space of $E - L - L_z$. We chose this space because the satellite's internal substructure (due to the presence of individual streams) is less well defined and, therefore, is more suitable for a clustering search of global structures. Enclosed in this sphere we find a total of $\sim 8 \times 10^4$ stellar particles, coming from 26 different satellites contributing each with at least 20 particles. In addition, the disc and the bulge contribute with $\sim 20\,000$ and ~ 2000 particles, respectively. For this analysis we deliberately chose to sample a larger volume of physical space so that each satellite is represented with a larger number of stellar particles. In this way, we can avoid overfragmentation, which occurs when a clump is populated with a very small number of particles.

Fig. 11 shows the different clusters of particles identified with this method. We have found 17 groups that contain more than 20 particles. Out these 17 groups, only 15 have more than 50 per cent of their particles associated to a single progenitor. One of these groups corresponds to the disc while two others are double detections of two different satellites that were fragmented by the algorithm. Therefore, only 12 of these groups can be uniquely associated to a single satellite. This corresponds to ~ 50 per cent of all the satellites contributing with stars to this volume. This is a similar recovery rate to that obtained by Helmi & de Zeeuw (2000), but now under a more realistic cosmological model and with the latest model for the *Gaia* measurement errors.

When attempting to compute the time since accretion, we were successful only in four cases. These groups are indicated in Fig. 11 with black open circles. Two of them correspond to the satellites labelled number 1 and 2 in previous analysis. In general, we find that the remaining identified groups lack a significant number of 'stars' with the required relative parallax error, $\sigma_\varpi/\varpi \leq 0.02$ (i.e. typically ≤ 50). However, as explained before, in this simulation our limited numerical resolution led us to consider only stars with $M_V \leq 4.5$. After estimating the number of stellar particles within 1 kpc from the Sun that may be observed by *Gaia* with the required
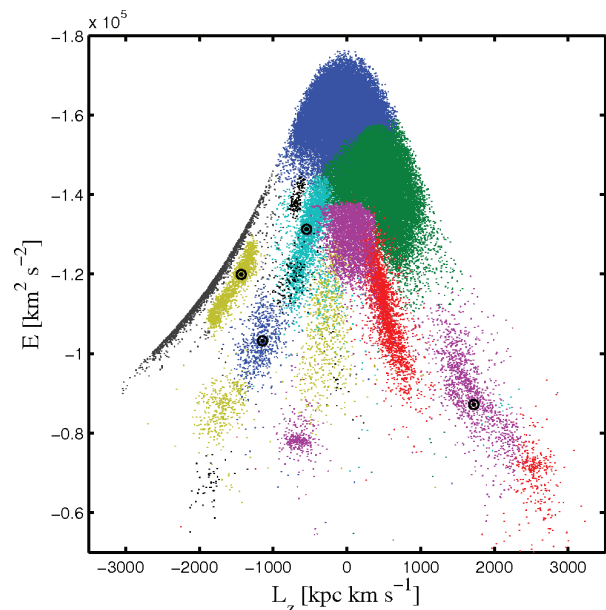

Figure 11. Distribution of stellar particles inside a sphere of 4-kpc radius at 8 kpc from the galactic centre in E versus L_z space as would be observed by *Gaia*. The different colours show the groups identified by the mean shift algorithm. Black open circles denote those for which the time since accretion was successfully derived.

[4] In this derivation we have assumed that relative errors in proper motion are of the same order of magnitude as those in the parallax. However, for the *Gaia* mission the former are expected to be in general an order of magnitude smaller.

© 2010 The Authors. Journal compilation © 2010 RAS, MNRAS **408**, 935–946

relative parallax errors (as explained in Section 4.2.1), we find that at least two additional satellites, among the 12 previously isolated, should have at least 200 stellar particles available to compute a reliable power spectrum.

5 SUMMARY AND CONCLUSIONS

We have studied the characteristics of merger debris in the solar neighbourhood as may be observed by ESA's *Gaia* mission in the near future. We have run a suite of *N*-body simulations of the formation of the Milky Way stellar halo set-up to match, at the present time, its known properties such as the velocity ellipsoid, density profile and total luminosity. The simulations follow the accretion of a set of 42 satellite galaxies on to a semicosmological time-dependent Galactic potential. These satellites are evolved for 10 Gyr, and we use the final positions and velocities of the constituent particles to generate a mock *Gaia* catalogue.

Using synthetic CMDs, we have resampled the satellite's particles to represent stars down to $M_V \approx 4.5$. This absolute magnitude corresponds to an apparent magnitude $V \approx 16$ at 2.5 kpc, which is comparable to the *Gaia* magnitude limit for which full phase-space information will be available. Our mock catalogue also includes a Galactic background population of stars represented by a Monte Carlo model of the Galactic disc and bulge, as in BVA05. At 8 kpc from the Galactic centre, stars from the disc largely outnumber those of the stellar halo. However, it is possible to reduce their impact by applying a simple cut on metallicity. Using the latest determinations of the MDF of the Galactic disc(s) (Nordström et al. 2004; Ivezić et al. 2008) we have estimated that only 10 000 stars out of the estimated 4.1×10^7 disc stars brighter than $V = 17$ in the solar neighbourhood should have [Fe/H] ≤ -1.1. A smaller number of bulge stars ($\sim$800) with [Fe/H] ≤ -1.1 is expected to contaminate our stellar halo sample, down to the faintest M_V. This fraction represents only 2.6 per cent of the whole mock *Gaia* stellar halo catalogue, and therefore does not constitute an important obstacle to our ability to characterize this component.

Finally, we have convolved the positions and velocities of all 'observable stars' in our solar neighbourhood sphere with the latest models of the *Gaia* observational errors, according to performances given by ESA (http://www.rssd.esa.int/gaia).

The analysis presented here confirms previous results, namely that satellites can be identified as coherent clumps in phase space, e.g. in the $E - L_z$ projection (see Helmi & de Zeeuw 2000; Knebe et al. 2005; Font et al. 2006). We find that a clustering algorithm such as mean shift (Fukunaga & Hostetler 1975; Comaniciu & Meer 2002; Derpanis 2005) is able to recover roughly 50 per cent of all satellites contributing stellar particles to the solar neighbourhood sphere.

We have also demonstrated that even after accounting for the Galactic background contamination and the expected measurement errors for the *Gaia* mission, the space of orbital frequencies is also very rich in substructure. In this space streams from a given satellite define a regular pattern whose characteristic scale is determined by the satellite's time since accretion. We find that reasonable estimates of the time since accretion may be provided when the number of stars with accurate parallaxes ($\sigma_\varpi/\varpi \leq 0.02$) from a given satellite is at least $\sim$100. This was possible in our simulations for four cases.

In addition to *Gaia*, massive ground-based spectroscopic surveys are currently being planned by both the European astronomical community (see e.g. GREAT, http://www.ast.cam.ac.uk/GREAT/) and other non-European collaborations (e.g. LAMOST, Zhao et al. 2006; HERMES, Wylie-de Boer & Freeman 2010; APOGEE, Majewski et al. 2010; BigBOSS, Schlegel et al. 2009). For some of these projects (mostly those led by Europe) the goal is to complement a future *Gaia* catalogue with information that either will not be obtained or for which the accuracy will be low. As an example, multi-object spectroscopy of intermediate resolution could be used to push the limiting magnitude of the phase-space catalogue down to $V \approx 20$. In combination with accurate (photometric or trigonometric) parallaxes this would allow the identification of satellites in, e.g. $E - L_z$ space beyond the extended solar neighbourhood. First, very faint satellites could now be observed and, secondly, the much larger sample of stars could be used to apply a clustering algorithm in very small volumes around the Sun with enough resolution to avoid large overfragmentation. Furthermore, by extending the volume probed we expect to reduce the overlap between satellites in $E - L_z$ space. In addition, a multi-object spectrograph with a high-resolution $R \gtrsim 20\,000$ mode would provide detailed chemical abundance patterns of individual stars. This could be used to characterize the satellite's star formation and chemical histories, and opens up the possibility of performing 'chemical tagging' (Freeman & Bland-Hawthorn 2002). Note, however, that in our simulations we find that stellar particles in a given stream do not originate from a localized region in physical space (such as a single molecular cloud). Therefore even individual streams are likely to reflect the full MDF present in the object at the time it was accreted.

Although our satellites were evolved in a cosmologically motivated time-dependent host potential, our simulations do not contain the fully hierarchical and often chaotic build-up of structure characteristic of the ΛCDM model. The violent variation of the host potential during merger events, the chaotic behaviour induced by a triaxial dark matter halo (e.g. Vogelsberger et al. 2008), and the orbital evolution due to baryonic condensation (Valluri et al. 2010), are potentially important effects which we have neglected and should be taken into account in future work. To assess the impact of some of these effects on the distribution of debris in the solar neighbourhood we are currently analysing fully cosmological high-resolution simulation of the formation of galactic stellar haloes based on the Aquarius project (Cooper et al. 2010).

REFERENCES

Allen C., Santillán A., 1991, Revista Mexicana Astron. Astrofísica, 22, 255
Aparicio A., Gallart C., 2004, AJ, 128, 1465
Arifyanto M. I., Fuchs B., 2006, A&A, 449, 533
Belokurov V. et al., 2006, ApJ, 642, L137
Belokurov V. et al., 2007, ApJ, 658, 337
Brown A. G. A., Velásquez H. M., Aguilar L. A., 2005, MNRAS, 359, 287 (BVA05)
Bryan G., Norman M., 1998, ApJ, 495, 80
Bullock J. S., Johnston K. V., 2005, ApJ, 635, 931
Carpintero D. D., Aguilar L. A., 1998, MNRAS, 298, 1

Cole S., Aragon-Salamanca A., Frenk C. S., Navarro J. F., Zepf S. E., 1994, MNRAS, 271, 781

Cooper A. P. et al., 2010, MNRAS, 406, 744

De Lucia G., Helmi A., 2008, MNRAS, 391, 14

Derpanis K. G., 2005, available online, http://www.cse.yorku.ca/∼kosta/CompVis_Notes/mean_shift.pdf

Font A. S., Johnston K. V., Bullock J. S., Robertson B. E., 2006, ApJ, 646, 886

Freeman K., Bland-Hawthorn J., 2002, ARA&A, 40, 487

Fuchs B., Jahreiß H., 1998, A&A, 329, 81

Fukunaga K., Hostetler L., 1975, IEEE Trans. Inf. Theory, 21, 3240

Gómez F. A., Helmi A., 2010, MNRAS, 401, 2285 (GH10)

Grillmair C. J., 2006, ApJ, 645, L37

Guzmán R., Lucey J. R., Bower R. G., 1993, MNRAS, 265, 731

Helmi A., 2008, A&AR, 15, 145

Helmi A., de Zeeuw P. T., 2000, MNRAS, 319, 657

Helmi A., White S. D. M., 1999, MNRAS, 307, 495

Helmi A., White S. D. M., de Zeeuw P. T., Zhao H., 1999, Nat, 402, 53

Helmi A., White S. D. M., Springel V., 2003, MNRAS, 339, 834

Helmi A., Navarro J. F., Nordström B., Holmberg J., Abadi M. G., Steinmetz M., 2006, MNRAS, 365, 1309

Hernquist L., 1990, ApJ, 356, 359

Høg E. et al., 2000, A&A, 355, L27

Ibata R. A., Gilmore G., Irwin M. J., 1994, Nat, 370, 194

Ibata R. A., Irwin M. J., Lewis G. F., Ferguson A. M. N., Tanvir N., 2001a, Nat, 412, 49

Ibata R. A., Irwin M. J., Lewis G. F., Stolte A., 2001b, ApJ, 547, L133

Ibata R., Irwin M. J., Lewis G. F., Ferguson A. M. N., Tanvir N., 2003, MNRAS, 340, L21

Ivezić Ž. et al., 2008, ApJ, 684, 287

King I. R., 1966, AJ, 71, 64

Klement R. et al., 2009, ApJ, 698, 865

Knebe A., Gill S., Kawata D., Gibson B. K., 2005, MNRAS, 357, 35

Koposov S. et al., 2008, ApJ, 686, 279

Kroupa P., Tout C. A., Gilmore G., 1993, MNRAS, 262, 545

McConnachie A. W. et al., 2009, Nat, 461, 6673

McMillan P. J., Binney J., 2008, MNRAS, 390, 429

Majewski S. R., Skrutskie M. F., Weinberg M. D., Ostheimer J. C., 2003, ApJ, 599, 1082

Majewski S. R., Wilson J. C., Hearty F., Schiavon R. R., Skrutskie M. F., 2010, in Cunha K., Spite M., Barbuy B., eds, Proc. IAU Symp. 265, Cambridge University Press, Cambridge, p. 480

Marigo P., Girardi L., Bressan A., Groenewegen M. A. T., Silva L., Granato G. L., 2008, A&A, 482, 883

Martínez-Delgado D. et al., 2008, ApJ, 689, 184

Martínez-Delgado D., Pohlen M., Gabany R. J., Majewski S. R., Peñarrubia J., Trujillo I., 2009, ApJ, 692, 955

Mihalas D., Binney J., 1981, Galactic Astronomy: Structure and Kinematics, 2nd edn. Freeman & Co., New York

Miyamoto M., Nagai R., 1975, PASJ, 27, 533

Navarro J. F., Frenk C. S., White S. D. M., 1996, ApJ, 462, 563

Newberg H. J. et al., 2002, ApJ, 569, 245

Nordström B. et al., 2004, A&A, 418, 989

Perryman M. A. C. et al., 1997, A&A, 323, 49

Perryman M. A. C. et al., 2001, A&A, 369, 339

Pietrinferni A., Cassisi S., Salaris M., Castelli F., 2004, ApJ, 612, 168

Plummer H. C., 1911, MNRAS, 71, 460

Schlegel D. J. et al., 2009, preprint (arXiv:0904.0468)

Schuster W. J., Allen C., 1997, A&A, 319, 796

Sharma S., Johnston K. V., 2009, ApJ, 703, 1061

Smith M. C. et al., 2007, MNRAS, 379, 755

Smith M. C. et al., 2009, MNRAS, 399, 1223

Sofue Y., Honma M., Omodaka T., 2009, PASJ, 61, 227

Springel V., 2005, MNRAS, 364, 1105

Starkenburg E. et al., 2009, ApJ, 698, 567

Tumlinson J., 2010, ApJ, 708, 1398

Valluri M., Debattista V. P., Quinn T., Moore B., 2010, MNRAS, 403, 525

Vogelsberger M., White S. D. M., Helmi A., Springel V., 2008, MNRAS, 385, 236

Wechsler R. H., Bullock J. S., Primack J. R., Kravtsov A. V., Dekel A., 2002, ApJ, 568, 52

White S. D. M., Rees M. J., 1978, MNRAS, 183, 341

White S. D. M., Springel V., 2000, in Weiss A., Abel T. G., Hill V., eds, The First Stars. Springer, Berlin, p. 327

Wylie-de Boer E., Freeman K., 2010, in Cunha K., Spite M., Barbuy B., eds, Proc. IAU Symp. 262, Cambridge University Press, Cambridge, p. 448

Yanny B. et al., 2003, ApJ, 588, 824

Yanny B. et al., 2009, AJ, 137, 4377

Zhao D. H., Mo H. J., Jing Y. P., Börner G., 2003, MNRAS, 339, 12

Zhao G., Chen Y., Shi J., Liang Y., Hou J., Chen L., Zhang H., Li A., 2006, Chinese J. Astron. Astrophys., 6, 265

Zoccali M., 2010, in Cunha K., Spite M., Barbuy B., eds, Proc. IAU Symp. 265, Cambridge University Press, Cambridge, p. 271

Zwitter T. et al., 2008, AJ, 136, 421

This paper has been typeset from a TEX/LATEX file prepared by the author.